Neural Comput & Applic (2009) 18:591–602
DOI 10.1007/s00521-009-0246-2

ORIGINAL ARTICLE

Local excitation solutions in one-dimensional neural fields by external input stimuli

Shigeru Kubota · Kosuke Hamaguchi · Kazuyuki Aihara

Received: 1 January 2007 / Accepted: 1 June 2008 / Published online: 24 February 2009

Abstract Cortical neurons are massively connected with other cortical and subcortical cells, and they receive synaptic inputs from multiple sources. To explore the basis of how interconnected cortical cells are locally activated by such inputs, we theoretically analyze the local excitation patterns elicited by external input stimuli by using a one-dimensional neural field model. We examine the conditions for the existence and stability of the local excitation solutions under arbitrary time-invariant inputs and establish a graphic analysis method that can detect all steady local excitation solutions and examine their stability. We apply this method to a case where a pair of supra- and subthreshold stimuli are applied to nearby positions in the field. The results demonstrate that there can exist bistable local excitation solutions with different lengths and that the local excitation exhibits hysteretic behavior when the relative distance between the two stimuli is altered.

S. Kubota (✉)
Department of Bio-System Engineering, Yamagata University, 4-3-16 Jonan, Yonezawa, Yamagata 992-8510, Japan
e-mail: kubota@yz.yamagata-u.ac.jp

K. Hamaguchi
RIKEN Brain Science Institute, 2-1 Hirosawa, Wako, Saitama 351-0198, Japan

K. Aihara
Institute of Industrial Science, University of Tokyo, 4-6-1 Komaba, Meguro-ku, Tokyo 153-8505, Japan

K. Aihara
ERATO Aihara Complexity Modelling Project, JST, 4-6-1 Komaba, Meguro-ku, Tokyo 153-8505, Japan

Keywords Neural field · Local excitation · Pattern formation · Neuroscience

1 Introduction

Local cortical areas are massively connected with other brain structures, including both cortical and subcortical areas, and neuronal information processing in the cortex is performed by receiving synaptic inputs from multiple sources. In this study, we thus consider the firing response of the cortical neurons that receive input stimuli, by using a neural field model that describes the large-scale dynamics of the densely distributed cortical neurons.

Pattern formation in neural fields is a research topic receiving ongoing interest, and a number of studies have analyzed neural field dynamics from various aspects (e.g., [1–17]). These studies have explored the existence and stability of characteristic solutions such as local excitations or "bumps" [1–9], traveling fronts or waves [1, 2, 7, 10–12], as well as the global convergence when the system starts from arbitrary initial conditions [13–15] (for reviews, see [16, 17]). While many studies have concerned pattern formation in the absence of external inputs or with constant or unimodal inputs, Wilson and Cowan [1] and Enculescu and Bestehorn [6] have examined how two adjacent input stimuli can be fused into localized activity and have found the existence of spatial hysteresis in pattern dynamics when the two inputs are moved slowly. Their results have shown that some type of hysteresis observed in the sensory perception [18] could probably arise from the interaction of sensory stimuli with intracortical excitation and inhibition. However, it is still not fully understood how various sensory stimuli to the cortex can be fused into localized activity via the interaction between neurons.

Therefore, in the present study, we theoretically analyze how external input stimuli can yield localized excitation by using the Amari-type one-dimensional neural field model [2]. We provide the conditions for the existence and stability of local excitation solutions and propose a graphic analysis method that can detect the steady local excitation solutions and examine their stability. The paper is organized as follows. In Sects. 2 and 3, we analyze the conditions for the existence and stability of localized solutions, respectively. In Sect. 4, we show that these conditions are described as the relationships between several characteristic functions and propose the graphic analysis method. In Sect. 5, we apply this method to a neural field receiving a pair of supra- and subthreshold stimuli and demonstrate that two stable local excitation solutions can coexist. It is also shown here that when the distance between the two stimuli are altered, we can find hysteretic pattern dynamics with respect to the length of local excitation, which is different from the hysteresis demonstrated in previous studies [1, 6]. We conclude in Sect. 6 with a discussion.

2 Local excitation solutions in neural fields

We consider the following one-dimensional neural field model [2].

$$\tau \frac{\partial u(x,t)}{\partial t} = -u(x,t) + \int w(x-x')f[u(x',t)]\mathrm{d}x' + S(x) - h, \tag{1}$$

where $u(x)$ is the average membrane potential of neurons at position x, τ is the time constant, $w(x-x')$ is the connectivity function from neurons at position x' to ones at position x, $f(u)$ is the output function, and $S(x)$ is the time-invariant input stimuli applied to the neurons at position x, and $-h(h>0)$ is the resting potential.

We consider the field with symmetric connections that are excitatory for proximate neurons so that $w(x)$ satisfies $w(x) = w(-x)$ and $w(0) > 0$. Unless otherwise stated, $f(u)$ is assumed to be a step function, i.e., $f(u) = 0$ for $u \leq 0$ and $f(u) = 1$ otherwise. As in Amari [2], let $R[u] = \{x|u(x) > 0\}$ be the excited region. Then, a local excitation of length $x_2 - x_1$ is defined as the state of the membrane potential distribution with $R[u] = (x_1, x_2)$.

We first examine the conditions where a steady local excitation solution with $R[u] = (x_1^*, x_2^*)$ can exist when arbitrary stationary input $S(x)$ is given. We introduce two characteristic functions: $W(x) = \int_0^x w(x')\mathrm{d}x'$ and $G(x) \equiv G[x; x_1^*, x_2^*] = -W(x-x_1^*) + W(x-x_2^*) + h$. Then, we see $W(0) = 0$ and $W(x) = -W(-x)$. We can also find the relation of the two functions:

$$G(x_1^*) = G(x_2^*) = -W(x_2^* - x_1^*) + h. \tag{2}$$

Since $\partial u/\partial t = 0$ in (1) at equilibrium, the membrane potential distribution at the steady state is given as $\bar{u}(x) = \int_{R[\bar{u}]} w(x-x')\mathrm{d}x' + S(x) - h$. Hence, the steady solution of local excitation with $R[u] = (x_1^*, x_2^*)$ is

$$\bar{u}(x) = W(x-x_1^*) - W(x-x_2^*) + S(x) - h. \tag{3}$$

The conditions for the existence of steady local excitation solutions are given by the following theorem:

Theorem 1 *There exists a steady solution of local excitation with $R[u] = (x_1^*, x_2^*)$ if and only if $S(x)$ and $G(x)$ satisfy the following three conditions*:

steady condition 1

$$S(x) = G(x), \quad \text{if } x = x_1^*, x_2^*, \tag{4}$$

steady condition 2

$$S(x) > G(x), \quad \text{if } x_1^* < x < x_2^*, \tag{5}$$

steady condition 3

$$S(x) < G(x), \quad \text{if } x < x_1^*, x_2^* < x. \tag{6}$$

Proof of Theorem 1 If there is a steady local excitation solution with $R[u] = (x_1^*, x_2^*)$, $\bar{u}(x)$ in (3) satisfies $\bar{u}(x_1^*) = \bar{u}(x_2^*) = 0$. This yields $S(x_1^*) = S(x_2^*) = -W(x_2^* - x_1^*) + h$, so that we obtain (4) by using (2). $\bar{u}(x)$ also satisfies $\bar{u}(x) > 0$ for $x_1^* < x < x_2^*$ and $\bar{u}(x) > 0$ for $x < x_1^*, x_2^* < x$. These relations can be transformed into (5) and (6).

On the contrary, if (4)–(6) hold, we can prove that $u(x) = S(x) - G(x)$ is a required steady local excitation solution for $R[u] = (x_1^*, x_2^*)$. □

The theorem indicates that relation between the external input $S(x)$ and the characteristic function $G(x)$ determines whether a steady local excitation solution exists. For the existence of a steady local excitation solution, $S(x)$ must be larger than $G(x)$ only inside the boundaries of the local excitation, and smaller outside the excitation. The proof of the theorem shows that the physical meaning of the characteristic function $G(x)$ is understood such that $u(x) = S(x) - G(x)$ becomes a steady membrane potential distribution for the local excitation. We refer to (4), (5), and (6) as the steady conditions 1, 2, and 3, respectively. This theorem is used to find steady solutions of local excitation below in the discussion about the graphic analysis method.

3 Stability of local excitation solutions

This section examines the stability of a steady local excitation solution with $R[u] = (x_1^*, x_2^*)$. We reduce the neural field equation (1) to an ordinary differential equation with respect to the boundaries of the excited region by the approach similar to [2, 5].

Assume that the membrane potential distribution with $R[u] = (x_1, x_2)$ at time t has changed to that of $R[u] = (x_1 + \mathrm{d}x_1, x_2 + \mathrm{d}x_2)$ at time $t + \mathrm{d}t$. Then, we can obtain the motion of the boundaries of the excited region just like [2]:

$$\frac{dx_i}{dt} = -\frac{1}{\tau u_{xi}}\{W(x_2 - x_1) + S(x_i) - h\}, \quad i = 1, 2, \tag{7}$$

where u_{xi} denotes $\partial u(x_i,t)/\partial x$. Let us consider small perturbations $\tilde{x}_i$ and $\tilde{u}_{xi}$ in x_i and u_{xi}, respectively. Then, if we substitute $x_i = x_i^* + \tilde{x}_i$ and $u_{xi} = u_{xi}^* + \tilde{u}_{xi}$ into the above equation and neglect the second and higher order terms of the perturbations, we can obtain a linear differential equation with respect to the boundaries x_1, x_2 of the excited region:

$$\frac{\mathrm{d}}{\mathrm{d}t}\begin{bmatrix}\tilde{x}_1\\ \tilde{x}_2\end{bmatrix} = \frac{1}{\tau}\begin{bmatrix}\{w(a^*) - S_{x1}^*\}/u_{x1}^* & -w(a^*)/u_{x1}^*\\ w(a^*)/u_{x2}^* & -\{w(a^*) + S_{x2}^*\}/u_{x2}^*\end{bmatrix}\begin{bmatrix}\tilde{x}_1\\ \tilde{x}_2\end{bmatrix}, \tag{8}$$

where $a^* \equiv x_2^* - x_1^*$ is the length of the steady local excitation. $u_{xi}^* \equiv \mathrm{d}\bar{u}(x_i^*)/\mathrm{d}x$ and $S_{xi}^* \equiv \mathrm{d}S(x_i^*)/\mathrm{d}x$ denote the gradients of the steady membrane potential distribution and the external inputs. The characteristic equation of the matrix in (8) is given by $\lambda^2 + B\lambda + C = 0$, where

$$B = \frac{1}{\tau}\left(-\frac{w(a^*) - S_{x1}^*}{u_{x1}^*} + \frac{w(a^*) + S_{x2}^*}{u_{x2}^*}\right), \tag{9}$$

$$C = \frac{1}{\tau^2 u_{x1}^* u_{x2}^*}\left\{w(a^*)(S_{x1}^* - S_{x2}^*) + S_{x1}^* S_{x2}^*\right\}. \tag{10}$$

By analyzing the eigenvalues of the characteristic equation, we obtain the following theorem:

Theorem 2 *A steady solution of local excitation with* $R[u] = (x_1^*, x_2^*)$ *is*

(1) *stable if* $S_{x1}^* > S_{x2}^*$ *and* $w(a^*)(S_{x1}^* - S_{x2}^*) + S_{x1}^* S_{x2}^* < 0$,
(2) *unstable if* $S_{x1}^* < S_{x2}^*$ *or* $w(a^*)(S_{x1}^* - S_{x2}^*) + S_{x1}^* S_{x2}^* > 0$.

The proof is given in Appendix A. It should be noted that, in the limit of $S_{x1}^*, S_{x2}^* \to 0$ with $S_{x1}^* > S_{x2}^*$, the theorem agrees with the stability conditions for homogeneous inputs [2].

4 Graphic analysis method

For the practical purpose, what matters is how we can actually find the stable and unstable steady solutions. Here we construct a graphic analysis method to find the steady local excitation solutions and examine their stability from the intersections and gradients of several characteristic curves.

4.1 Description of the steady condition 1 by the characteristic curves

Definition 1 *We define the* $a - \hat{S}$ *curve to be a set of points* $(a, \hat{S})$ *in the plane spanned by* a *and* $\hat{S}$ *such that there exist* x_1 *and* x_2 *satisfying the three conditions: (1)* $x_1 < x_2$, *(2)* $S(x_1) = S(x_2) = \hat{S}$, *and (3)* $a = x_2 - x_1$.

Figure 1a, b illustrates a simple example of $S(x)$ and the corresponding $a - \hat{S}$ curve. Note that the function $S(x)$ is arbitrary and does not need to be unimodal as in the figure. The method for plotting the $a - \hat{S}$ curve is not instructive, but rather complex, so that the method is given in Appendix B.

Let us define another characteristic function $Y(a)$ to be

$$Y(a) = h - W(a). \tag{11}$$

Then, the following theorem shows that, if the $a - \hat{S}$ curve is plotted with function $Y(a)$ on the same plane as shown in Fig. 1c, an intersection of both curves corresponds to a solution of the steady condition 1 in Theorem 1.

Theorem 3 *The steady condition 1 holds for* x_1^*, x_2^* $(x_1^* < x_2^*)$ *if and only if* $S(x_1^*) = S(x_2^*)$ *and the point* (a^*, S^*) *with* $a^* = x_2^* - x_1^*$ *and* $S^* = S(x_1^*) = S(x_2^*)$ *lies on an intersection of the* $a - \hat{S}$ *curve with* $Y(a)$.

Proof of Theorem 3 When the steady condition 1 holds, $S(x_1^*) = S(x_2^*)$ also holds from (2). Thus, from Definition 1, the point (a^*, S^*) with $a^* = x_2^* - x_1^*$ and $S^* = S(x_1^*) = S(x_2^*)$ lies on the $a - \hat{S}$ curve. We can also find the following relation by using (2) and the steady condition 1:

$$Y(a^*) = h - W(x_2^* - x_1^*) = S^*, \tag{12}$$

so that the point (a^*, S^*) lies on the curve $Y(a)$. Hence, the point (a^*, S^*) lies on an intersection of the $a - \hat{S}$ curve and $Y(a)$.

On the contrary, if $S(x_1^*) = S(x_2^*)$ holds and the point (a^*, S^*) with $a^* = x_2^* - x_1^*$ and $S^* = S(x_1^*) = S(x_2^*)$ lies on an intersection of the two curves, then (12) holds so that we obtain the steady condition 1 from (2). □

Theorem 3 will be used below for finding the solutions satisfying the steady condition 1 from the intersections of the $a - \hat{S}$ curve with $Y(a)$. Note that, since the steady conditions 2 and 3 are not taken into account in Theorem 3, relation between the two curves are not enough to find the steady local excitation solutions. However, the gradient of the $a - \hat{S}$ curve and $Y(a)$ gives another useful information about the stability condition as follows.

4.2 Description of the stability condition by the characteristic curves

Let us assume that a local excitation with $R[u] = (x_1^*, x_2^*)$ exists. Then, we can find from Theorem 1 that the three

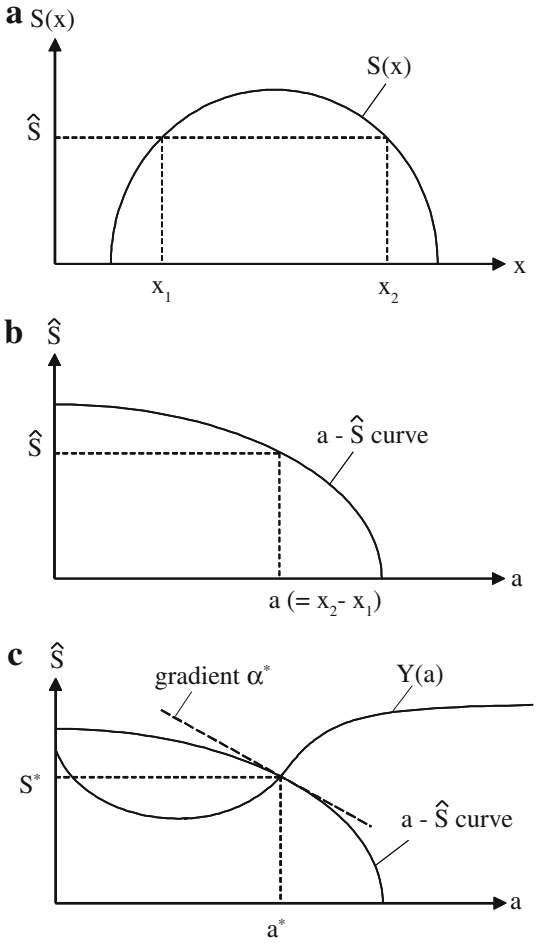

Fig. 1 A simple example of the $a - \hat{S}$ curve and the definition of α^* (**a**, **b**). External input stimuli $S(x)$ (**a**) and the corresponding $a - \hat{S}$ curve (**b**), where the four variables x_1, x_2, a, and $\hat{S}$ satisfy the three conditions in Definition 1. **c** The $a - \hat{S}$ curve and $Y(a)$. α^* is defined as the gradient of the $a - \hat{S}$ curve at the intersection point (a^*, S^*) of these curves

steady conditions are satisfied, and from Theorem 3 that the point (a^*, S^*) with $a^* = x_2^* - x_1^*$ and $S^* = S(x_1^*) = S(x_2^*)$ lies on an intersection of the $a - \hat{S}$ curve and $Y(a)$. As shown in Fig. 1c, we define $\alpha^*(\equiv \mathrm{d}\hat{S}(a^*)/\mathrm{d}a)$ to be the gradient of the $a - \hat{S}$ curve at the intersection.

Now we explore how the gradients of the characteristic curves $\mathrm{d}Y(a^*)/\mathrm{d}a$ and α^* are related to the stability of the local excitation solutions. Assume that x_1, x_2 $(x_1 < x_2)$, a, and $\hat{S}$, and their perturbations satisfy

$$S(x_1) = S(x_2) = \hat{S}, \tag{13}$$

$$S(x_1 + \Delta x_1) = S(x_2 + \Delta x_2) = \hat{S} + \Delta S, \tag{14}$$

$$a = x_2 - x_1, \tag{15}$$

$$a + \Delta a = (x_2 + \Delta x_2) - (x_1 + \Delta x_1). \tag{16}$$

Figure 2 shows the relationship of these variables with $S(x)$ and the corresponding $a - \hat{S}$ curve. The above equations

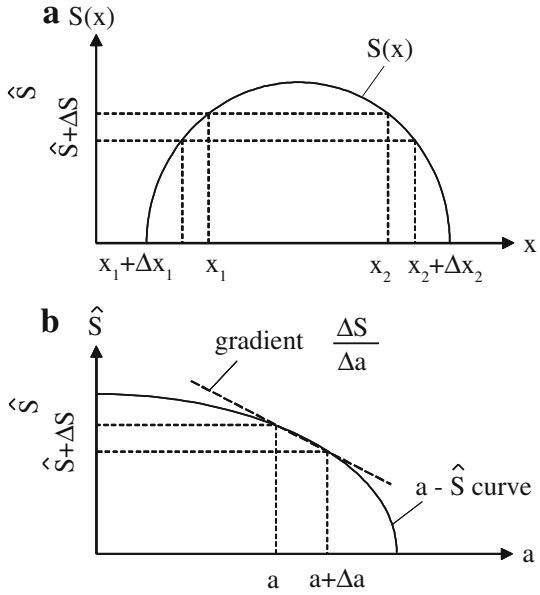

Fig. 2 Relationship among variables x_1, x_2, a, and $\hat{S}$, and their perturbations denoted by Δx_1, Δx_2, Δa, and ΔS that satisfy (13)–(16). The *solid curves* in **a** and **b** show $S(x)$ and the corresponding $a - \hat{S}$ curve

mean that both points $(a, \hat{S})$ and $(a + \Delta a, \hat{S} + \Delta S)$ lie on the $a - \hat{S}$ curve (Fig. 2b). The gradient of the line connecting the two points is given by

$$\frac{\Delta S}{\Delta a} = \frac{\Delta S}{\Delta x_2 - \Delta x_1} = \frac{\Delta S}{\Delta x_1} \cdot \frac{\Delta S}{\Delta x_2} \Big/ \left(\frac{\Delta S}{\Delta x_1} - \frac{\Delta S}{\Delta x_2} \right). \tag{17}$$

Hence, by taking the limit $\Delta S \to 0$ and setting $x_1 = x_1^*$, $x_2 = x_2^*$, and $a = a^*$, the gradient α^* of the $a - \hat{S}$ curve can be written in the following equation with $S_{xi}^* = \mathrm{d}S(x_i^*)/\mathrm{d}x$:

$$\alpha^* = \frac{\mathrm{d}\hat{S}(a^*)}{\mathrm{d}a} = \frac{S_{x1}^* S_{x2}^*}{S_{x1}^* - S_{x2}^*}. \tag{18}$$

Thus, the difference between the gradients of the two characteristic curves is

$$\begin{aligned} \frac{\mathrm{d}Y(a^*)}{\mathrm{d}a} - \alpha^* &= -w(a^*) - \frac{S_{x1}^* S_{x2}^*}{S_{x1}^* - S_{x2}^*} \\ &= -\frac{w(a^*)(S_{x1}^* - S_{x2}^*) + S_{x1}^* S_{x2}^*}{S_{x1}^* - S_{x2}^*}. \end{aligned} \tag{19}$$

Note that the terms in the fraction of the rightmost side also appear in the stability conditions in Theorem 2. Therefore, we can obtain the following theorem from Theorem 2 and (19).

Theorem 4 *A steady solution of local excitation with* $R[u] = (x_1^*, x_2^*)$ *is*

(1) *stable if* $S_{x1}^* > S_{x2}^*$ *and* $\mathrm{d}Y(a^*)/\mathrm{d}a > \alpha^*$,
(2) *unstable if* $S_{x1}^* < S_{x2}^*$ *or* $\mathrm{d}Y(a^*)/\mathrm{d}a < \alpha^*$.

This theorem indicates that the stability of a local excitation can be determined by the gradients of the characteristic curves and external inputs.

4.3 The proposed method

We can see from Theorem 3 that the solutions of the steady condition 1 correspond to the intersections of the $a - \hat{S}$ curve with $Y(a)$, and from Theorem 4 that the stability conditions can be expressed by the gradients of the characteristic curves. Here, we bring together these results and construct a graphic analysis method to find the steady solutions and their stability. The method is given below by the three steps. An example of applying the method is shown in the next section.

Step 1: **Finding the solutions of the steady condition 1** Plot the $a - \hat{S}$ curve by the method in Appendix B, and also plot the function $Y(a) = h - W(a)$ on the same plane. Let us denote the coordinates of all the intersection points of both curves by (a_k^*, S_k^*) $(k = 1,\ldots, M)$. Then, from Definition 1, there exist $x_{1,k}^*$ and $x_{2,k}^*$ that satisfy $a_k^* = x_{2,k}^* - x_{1,k}^*$ and $S(x_{1,k}^*) = S(x_{2,k}^*) = S_k^*$ for each k, so that we denote a set of $(x_{1,k}^*, x_{2,k}^*)$ by Θ_k. If we obtain Θ_k by the method in Appendix C, $(x_1^*, x_2^*) \in \bigcup_k \Theta_k$ become the solutions of the steady condition 1 from Theorem 3. (The detailed proof is given in Appendix C.)

Step 2: **Finding the steady solutions of local excitation** Plot $S(x)$ and $G[x; x_{1,k}^*, x_{2,k}^*]$ with $(x_{1,k}^*, x_{2,k}^*) \in \Theta_k$ on the same coordinate system for each k. Then, from the relation between the two curves, examine whether the steady conditions 2 and 3 hold according to Theorem 1. If all the steady conditions are satisfied, a steady local excitation solution with $R[u] = (x_{1,k}^*, x_{2,k}^*)$ exists from Theorem 1.

Step 3: **Examining stability of the steady local excitation solutions** Let α_k^* be the gradient of the $a - \hat{S}$ curve at the intersection point (a_k^*, S_k^*), and S_{x1}^* and S_{x2}^* be the gradient of $S(x)$ at $x = x_{1,k}^*$ and $x_{2,k}^*$. Then, from Theorem 4, a steady solution of local excitation with $R[u] = (x_{1,k}^*, x_{2,k}^*)$ is

(1) stable if $S_{x1}^* > S_{x2}^*$ and $\mathrm{d}Y(a_k^*)/\mathrm{d}a > \alpha_k^*$,
(2) unstable if $S_{x1}^* < S_{x2}^*$ or $\mathrm{d}Y(a_k^*)/\mathrm{d}a < \alpha_k^*$.

5 Bistability and hysteresis in local excitation

Now we apply the graphic analysis method in the previous section to the neural field receiving two nearby input stimuli. This input condition is motivated by the studies in Wilson and Cowan [1] and Enculescu and Bestehorn [6] that have shown the existence of hysteretic behavior in the field dynamics.

The previous studies [1, 6] have examined the field activity in the presence of two suprathreshold inputs with changing the relative distance between them as follows: first, the two inputs are applied to the same position, which leads to the excitation pattern of a single connected region. In the next step, the two stimuli are moved slowly to the opposite directions. Then, at a critical distance between the stimuli, the single excitation pattern is divided into two separated regions. Finally, the two inputs are moved again toward each other, and the two excited regions fuse at a critical distance. Their results show that the critical distance between the two inputs at which one excitation splits into two is larger than the critical distance at which the two excitations combine together.

Here we show that there exists a different type of hysteretic behavior with respect to the excited region of the local excitation when a pair of suprathreshold and subthreshold stimuli are used. We consider the input condition described as the sum of two unimodal inputs (Fig. 3a), i.e., $S(x) = S_A(x) + S_B(x)$, where $S_A(x) = \max[-0.3(x - x_A)^2 + 7.5,\ 0]$ and $S_B(x) = \max\left[-0.75(x - x_B)^2 + 3,\ 0\right]$. The stimulus threshold necessary for activation is set as $h = 6$ (red line in Fig. 3a), which means that $S_A(x)$ and $S_B(x)$ are suprathreshold and subthreshold inputs, respectively. The connectivity function $w(x)$ is assumed to be a lateral-inhibitory function: $w(x) = 2.8\exp[-x^2/(2 \cdot 3.9^2)] - 1.1\exp[-x^2/(2 \cdot 9.6^2)]$.

Figure 3 shows an example of applying the graphic analysis method for $x_A = 10$ and $x_B = 18$. Figure 3b shows the $a - \hat{S}$ curve (black lines) and $Y(a)$ (red reline) plotted on the same plane according to Step 1. Since there exist five intersections P_1 to P_5 of these curves, five sets of solutions $(x_{1,k}^*, x_{2,k}^*)$ (or Θ_k) for $k = 1,\ldots, 5$ satisfy the steady condition 1. These solutions are depicted by plotting the points $(x_{1,k}^*, S(x_{1,k}^*))$ and $(x_{2,k}^*, S(x_{2,k}^*))$ in Fig. 3c by open circles with corresponding number k, where the point $(x_{2,k}^*, S(x_{2,k}^*))$ is at the right side of $(x_{1,k}^*, S(x_{1,k}^*))$ for each k.

Figure 3c shows the functions $S(x)$ (black line) and $G[x; x_{1,k}^*, x_{2,k}^*](k = 1,\ldots, 5)$ (red lines) plotted according to Step 2, where $G[x; x_{1,k}^*, x_{2,k}^*]$ is denoted by G_k in the figure. Note that, the points $(x_{1,k}^*, S(x_{1,k}^*))$ and $(x_{2,k}^*, S(x_{2,k}^*))$ are intersections of $S(x)$ and $G[x; x_{1,k}^*, x_{2,k}^*]$ since $x_{1,k}^*$ and $x_{2,k}^*$ satisfy the steady condition 1. From Theorem 1, all the three steady conditions must be satisfied for the existence of a steady local excitation solution. This means that $S(x)$ must be greater than $G[x; x_{1,k}^*, x_{2,k}^*]$ only within a interval $(x_{1,k}^*, x_{2,k}^*)$. Since Fig. 3c indicates that the three steady conditions hold for $k = 3,4,5$ but not for $k = 1, 2$, we can understand that there exist three steady local excitation solutions with $R[u] = (x_{1,k}^*, x_{2,k}^*)$ $(k = 3, 4, 5)$. In the figure,

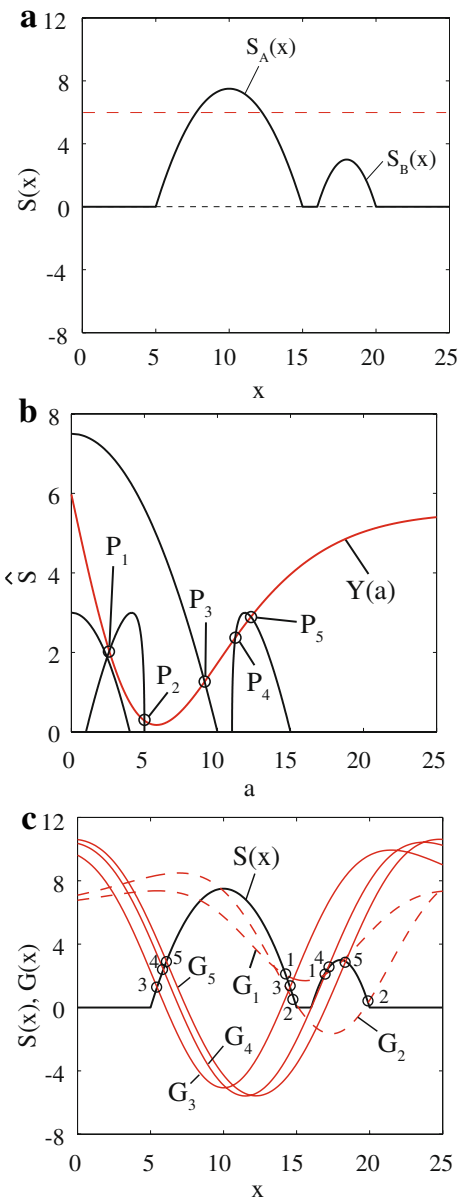

Fig. 3 An example of applying the graphic analysis method to the field with two adjacent inputs. **a** Input stimulus $S(x)$ is bimodal and composed of suprathreshold stimulus $S_A(x)$ and subthreshold stimulus $S_B(x)$. The *red horizontal line* shows the stimulus threshold (h) necessary for activation. **b** The $a - \hat{S}$ curve (*black*) and $Y(a)$ (*red*). The intersection points of the two curves are shown by the *open circles* labeled as $P_k(k = 1,\ldots, 5)$. **c** Functions $S(x)$ (*black*) and $G[x; x^*_{1,k}, x^*_{2,k}]$ ($k = 1,\ldots, 5$), which is labeled as G_k (*red*). The *open circles* show the points $(x^*_{1,k}, S(x^*_{1,k}))$ and $(x^*_{2,k}, S(x^*_{2,k}))$ with the corresponding number k. The point $(x^*_{1,k}, S(x^*_{1,k}))$ is on the left side of $(x^*_{2,k}, S(x^*_{2,k}))$ for each k. $G[x; x^*_{1,k}, x^*_{2,k}]$ is plotted by a *solid line* when all the steady conditions are satisfied for x^*_1 and x^*_2, and by a *dashed line* otherwise

$G[x; x^*_{1,k}, x^*_{2,k}]$ is plotted by a solid line when all the steady conditions are satisfied and by a dashed line otherwise.

Finally, according to Step 3, we examine the stability of the three steady local excitation solutions from Fig. 3b, c.

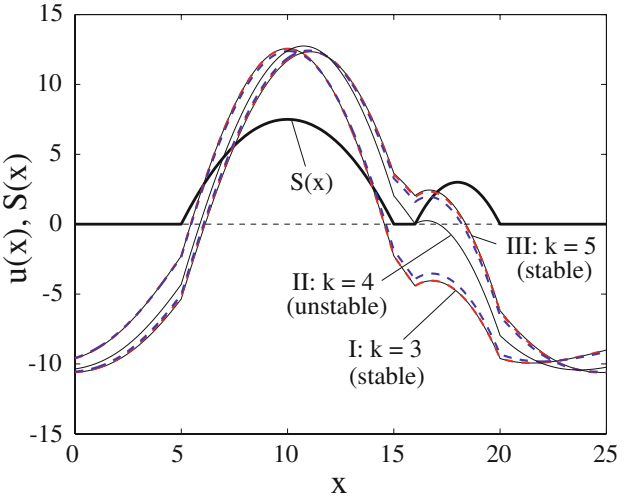

Fig. 4 Local excitation solutions obtained by the theory and numerical simulations. The *thin solid lines* show the steady membrane potential distribution $u(x)$ obtained by the graphic analysis method in Fig. 3, and the *dashed lines* depict the stable solutions found by the numerical simulation. The solutions for $k = 3$, 4, and 5 are those corresponding to the intersections P_3, P_4, and P_5 in Fig. 3b, respectively (see main text). In the simulation, the sigmoid output function $f(u) = 1/[1 + \exp(-u/\varepsilon)]$ is used with $\varepsilon = 0.5$ (*red*) and 1.5 (*blue*) for the solutions corresponding to $k = 3$, and with $\varepsilon = 0.1$ (*red*) and 0.5 (*blue*) for $k = 5$. Input stimulus $S(x)$ is shown by a *thick solid line*, which is the same as Fig. 3a. The solutions of $k = 3$, 5 are stable, whereas that of $k = 4$ is unstable. The results obtained by the theory and numerical simulations agree very well for small ε

In Fig. 3b, we compare the gradient α^*_k and $Y(a^*_k)/\mathrm{d}a$, i.e. the gradient of the $a - \hat{S}$ curve and that of curve $Y(a)$ at each intersection $P_k(k = 3, 4, 5)$. Then, we can find $\mathrm{d}Y(a^*_k)/\mathrm{d}a > \alpha^*_k$ for $k = 3$, 5 and $\mathrm{d}Y(a^*_k)/\mathrm{d}a < \alpha^*_k$ for $k = 4$. In Fig. 3c, we can compare S^*_{x1} and S^*_{x2} that are the gradient of $S(x)$ at the points $(x^*_{1,k}, S(x^*_{1,k}))$ and $(x^*_{2,k}, S(x^*_{2,k}))$ denoted by the open circles. Then, we find $S^*_{x1} > S^*_{x2}$ for $k = 3$, 4, 5. Thus, we have $\mathrm{d}Y(a^*_k)/\mathrm{d}a > \alpha^*_k$ and $S^*_{x1} > S^*_{x2}$ for $k = 3$, 5 and $\mathrm{d}Y(a^*_k)/\mathrm{d}a < \alpha^*_k$ and $S^*_{x1} > S^*_{x2}$ for $k = 4$. Therefore, we see from Theorem 4 that the steady local excitation solutions of $R[u] = (x^*_{1,k}, x^*_{2,k})$ are stable for $k = 3$, 5 and unstable for $k = 4$.

In Fig. 4, the membrane potential distribution $u(x)$ for the three steady local excitation solutions are plotted by using (3) (thin solid lines) with the results of the numerical simulations (dashed lines). In order to examine whether similar results can be obtained for the continuous output function case, we have used a sigmoid output function $f(u) = 1/[1 + \exp(-u/\varepsilon)]$ with changing the values of ε in the simulations. While our method is exact for the limit of $\varepsilon \to 0$, it provides good approximations for the cases with small ε. It should be noted that the argument here suggests the requirement of relatively long interaction lengths between neurons for the existence of bistable solutions. The interaction range much shorter than the length of input

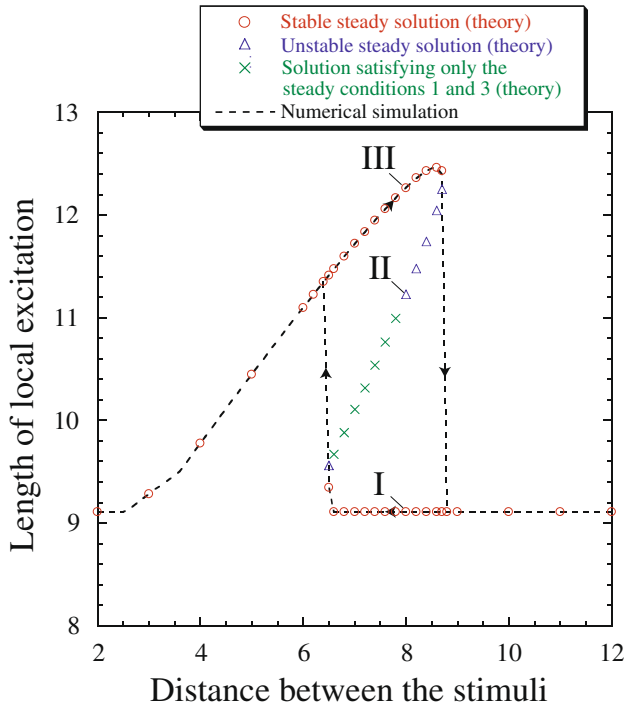

Fig. 5 Hysteresis in local excitation. The length of local excitation $a = x_2 - x_1$ has been investigated by changing the distance $D = x_B - x_A$ between the two inputs $S_A(x)$ and $S_B(x)$ in Fig. 3a. The *dashed lines* with *arrows* are the result of numerical simulation where the sigmoid output function ($\varepsilon = 0.1$) is used. The three types of symbols show the theoretical results of the graphic analysis method. Each *open circle* and *triangle* indicates the length of a stable and unstable steady local excitation solution, respectively. The × mark corresponds to the solutions that satisfy the steady conditions 1 and 3 in Theorem 1, but not the steady condition 2. The steady membrane potential distributions $u(x)$ for the solutions denoted by I, II, and III are the same as those in Fig. 4

stimuli, in which $w(x)$ converges to 0 at smaller x, leads to the disappearance of the stable and unstable intersection points in Fig. 3b (P_5 and P_4, respectively), which are required for the bistable solutions.

Since the bistable solutions seem to suggest the existence of hysteresis, we have examined the field activity by moving the two inputs like the previous studies [1, 6] (Fig. 5). The dashed lines depict the results of simulation, and show the length of local excitation $a = x_2 - x_1$ when the distance between the two inputs $D = x_B - x_A$ is slowly changed. The distance D is first increased from 0 to 12, and then decreased again from 12 to 0. The figure shows that, when D is within a certain range, there exist bistable local excitation solutions and the length of local excitation is large for the separating input case (increasing D) compared to the merging input case (decreasing D). This hysteretic behavior has been theoretically analyzed by applying the graphic analysis method as shown in the symbols in Fig. 5. The theoretical results show the existence of a continuous set of several types of solutions. When the distance D between the stimuli is either sufficiently large or small, there exists only one stable local excitation solution (circle). However, within the bistable range of D, the solution bifurcates into (1) two stable steady local excitation solutions (circle), and (2) either an unstable steady local excitation solution (triangle) or a solution satisfying only the steady conditions 1 and 3 (× mark). Note that, in cases where the steady condition 2 is not satisfied, we cannot obtain the corresponding local excitation solution. However, we can plot the value of $a^* = x_2^* - x_1^*$ from the solutions x_1^*, x_2^* satisfying the steady condition 1. It should be emphasized that, when unstable steady solutions disappear within the bistable range of D, hidden solutions satisfying only two of three steady conditions connect the unstable solutions to shape a continuous line. The continuity of these solutions results from Theorem 3, which indicates the existence of solutions satisfying at least the steady condition 1 corresponding to the intersections of the continuous characteristic curves. The membrane potential distribution $u(x)$ for the solutions I, II, and III in Fig. 5 are shown in Fig. 4 by using the same labels.

6 Discussion

Local excitation solutions have been analyzed in a one-dimensional neural field model in the presence of external inputs. By reducing the conditions for the existence and stability of the local excitation solutions into those for the intersections and gradients of the characteristic functions, we have proposed the graphic analysis method by which steady solutions and their stability can be found. We have applied this method to a neural field where both supra- and subthreshold stimuli are applied simultaneously, and have shown the existence of bistable local excitation solutions as well as the hysteretic behavior of the excited region.

Amari [2] has studied the local excitation solutions in a neural field with lateral-inhibitory connections and has fully analyzed the conditions for the existence and stability of solutions in the presence of spatially homogeneous inputs. We have extended the results of Amari to a case where the neural field receives inhomogeneous input stimuli. This extension is fundamental for exploring the response of cortical neurons, which are closely connected with other cortical and subcortical cells and receive the summation of various inputs at any time. The present analysis does not require specific assumptions with regard to the input function $S(x)$ as far as the function is time-independent; therefore, the existence and stability of localized solutions can be found for any stationary input pattern. Another characteristic feature of our analysis method is that it can detect the hidden solutions that satisfy only a part of the steady conditions in Theorem 1 and

cannot be obtained by numerical simulations (× mark in Fig. 5). This has enabled the elucidation of the geometrical structure of solutions for two moving inputs in Fig. 5, which shows that two branches of stable solutions are connected by the solutions comprised of unstable and hidden ones. Our results have also revealed the existence of bistable localized solutions with different lengths of excitation (Figs. 4, 5), which do not exist under homogeneous input conditions [2]. In more complicated input conditions (e.g., in the presence of three input stimuli), the graphic analysis method would predict an increase in the number of intersections between the $a - \hat{S}$ curve and $Y(a)$. Therefore, more than two stable local excitation solutions can also coexist.

The hysteretic pattern dynamics that we have shown is quite different from that reported in previous studies [1, 6]. Wilson and Cowan [1] and Enculescu and Bestehorn [6] have revealed the hysteretic pattern dynamics in one- and two-dimensional fields, respectively, when the relative distance between two suprathreshold stimuli is changed. On the other hand, in our model, the hysteresis dynamics has been elicited by using a pair of supra- and subthreshold stimuli. Additionally, in our case, hysteresis requires a relatively long interaction between neurons as mentioned above, which is not necessary for the hysteresis in the case of two suprathreshold stimuli [6]. This difference implies that these two types of hysteretic behavior may arise from different mechanisms of interplay between neurons. It will be a theoretically challenging problem to study how the qualitative feature of the field dynamics with two suprathreshold stimuli is different from or similar to the bifurcation diagram shown in Fig. 5. Furthermore, it is worth noting that the hysteresis dynamics in our model suggests a new experimental condition for inducing hysteresis in sensory perception. Previous studies [1, 6] have explained the perceptual hysteresis observed in the Fender-Julesz experiment [18] which shows that when the same images are presented to two eyes with changing retinal disparities, the disparity necessary for the breakaway of fused images is larger than that required for the refusion of the images. Based on our results, perceptual hysteresis may be induced when visual images such as bars are presented to one eye with a strong luminous intensity and to the other eye with a considerably weaker intensity. In this case, we predict that the subject would perceive that the width of the bar becomes larger when the retinal disparities of the images are increased than decreased within some range as shown in Fig. 5.

It has been suggested that the spatially localized excitation of cortical activity is correlated with several aspects of higher-level cognitive processing. The self-maintenance of local excitation has been proposed to underlie the persistent activity observed in the prefrontal cortex (PFC) neurons when an animal is holding items in working memory [19–23]. The involvement of local excitation in encoding sensory information is also supported by the observation that complex objects are represented by the spatial combination of active and inactive localized discharge pattern in the inferotemporal cortex (ITC) [24, 25]. These studies suggest that the appearance and disappearance of localized activity may be regulated in association cortices of PFC and ITC, which play a role in integrating feedforward inputs from multiple sensory areas. Therefore, the proposed method may be beneficial for understanding the basis of how localized neuronal discharge in association areas represents the information transmitted by the activity of lower-level cortical cells. Furthermore, the localized activity may be linked to neuronal responses in the head-direction neurons [26, 27] and feature selectivity in visual cortex cells [28]. To elucidate how these cell activities are modulated by the inputs from the environment, understanding of the behavior of localized excitation with external stimuli seems profitable. Several recent studies have also advanced the understanding of different types of localized solutions, such as the solutions whose excited region consists of $N \geq 2$ disjointed intervals [4, 5] and those in two-dimensional fields [3, 8], by using neural field models similar to ours. Thus, it would be intriguing to combine our results with these studies to analyze the existence and stability of stimulus-evoked excitations with disjointed intervals or study whether an extended method of graphic analysis is available for two-dimensional fields.

Acknowledgments This study is partially supported by the Advanced and Innovational Research Program in Life Sciences, Grant-in-Aid for Scientific Research on Priority Areas—System study on higher-order brain functions—(17022012), and the Grant-in-Aid for Scientific Research (KAKENHI (19700281), Young Scientists (B)) from the Ministry of Education, Culture, Sports, Science, and Technology, the Japanese Government. K. Hamaguchi is supported by JSPS Research Fellowship.

Appendix A: Proof of Theorem 2

(1) When $S^*_{x1} > S^*_{x2}$ and $w(a^*)\left(S^*_{x1} - S^*_{x2}\right) + S^*_{x1}S^*_{x2} < 0$ hold, we find $C > 0$ in (10) by using $u^*_{x1} > 0$ and $u^*_{x2} < 0$. Differentiating (3) with respect to x yields

$$\frac{\mathrm{d}\bar{u}(x)}{\mathrm{d}x} = w(x - x^*_1) - w(x - x^*_2) + \frac{\mathrm{d}S(x)}{\mathrm{d}x}. \tag{A.1}$$

Then, by substituting $x = x^*_1$ and x^*_2, we obtain

$$u^*_{x1} = w(0) - w(a^*) + S^*_{x1}, \tag{A.2}$$

$$u^*_{x2} = -w(0) + w(a^*) + S^*_{x2}. \tag{A.3}$$

From these equations, (9) can be transformed into

$$B = \frac{1}{\tau u^*_{x1} u^*_{x2}} \left[w(0)\left\{2w(a^*) - S^*_{x1} + S^*_{x2}\right\} - 2w(a^*)^2 + 2\left\{(S^*_{x1} - S^*_{x2})w(a^*) + S^*_{x1}S^*_{x2}\right\}\right]$$
$$= \frac{1}{\tau u^*_{x1} u^*_{x2}} \left[w(0)\left\{2w(a^*) - S^*_{x1} + S^*_{x2}\right\} - 2w(a^*)^2\right] + 2\tau C. \quad \text{(A.4)}$$

Hence, by using the relation

$$2w(a^*) - S^*_{x1} + S^*_{x2} < -\frac{2S^*_{x1}S^*_{x2}}{S^*_{x1} - S^*_{x2}} - S^*_{x1} + S^*_{x2} = -\frac{S^{*2}_{x1} + S^{*2}_{x2}}{S^*_{x1} - S^{*2}_{x2}} < 0 \quad \text{(A.5)}$$

and the property of the connectivity w(0) > 0, we can find $B > 0$. Therefore, both the coefficients B and C of the characteristic function are positive, so that the differential equation (8) is stable.

(2) When $w(a^*)\left(S^*_{x1} - S^*_{x2}\right) + S^*_{x1}S^*_{x2} > 0$ holds, we find $C < 0$ from (10) by using $u^*_{x1} > 0$ and $u^*_{x2} < 0$. Thus, the system is unstable.

Furthermore, when $S^*_{x1} > S^*_{x2}$ and $w(a^*)\left(S^*_{x1} - S^*_{x2}\right) + S^*_{x1}S^*_{x2} \le 0$ hold, we find

$$w(a^*) \ge -\frac{S^*_{x1}S^*_{x2}}{S^*_{x1} - S^*_{x2}}. \quad \text{(A.6)}$$

Hence,

$$w(a^*) - S^*_{x1} \ge -\frac{S^*_{x1}S^*_{x2}}{S^*_{x1} - S^*_{x2}} - S^*_{x1} = -\frac{S^{*2}_{x1}}{S^*_{x1} - S^*_{x2}} \ge 0, \quad \text{(A.7)}$$

$$w(a^*) + S^*_{x2} \ge -\frac{S^*_{x1}S^*_{x2}}{S^*_{x1} - S^*_{x2}} + S^*_{x2} = -\frac{S^{*2}_{x2}}{S^*_{x1} - S^*_{x2}} \ge 0. \quad \text{(A.8)}$$

Note that at least either S^*_{x1} or S^*_{x2} must take a value different from 0 because of $S^*_{x1} < S^*_{x2}$. Therefore, we obtain $B < 0$ from (9), so that the system is unstable.

Appendix B: The method for plotting the $a - \hat{S}$ curve

In this appendix, we show the method for plotting the $a - \hat{S}$ curve from the function $S(x)$ according to Definition 1. First, we give some definitions.

Definition 2 *We say that $f(x)$ is a monotone increasing (decreasing) function if $f(x_1) < f(x_2)$ ($f(x_1) > f(x_2)$) for any x_1, x_2 with $x_1 < x_2$ in its domain. We refer to a monotone increasing or decreasing function as a monotone function. We also say that $f(x)$ is a constant function if $f(x_1) = f(x_2)$ for any x_1 and x_2 in its domain.*

Definition 3 *We define $S_i(x)$ (i = 1,…, N) to be functions that satisfy the following three conditions, where a finite interval $[d_i, d_{i+1}]$ is the domain of $S_i(x)$. We refer to the function $S_i(x)$ as a subfunction of $S(x)$.*

(1) *$S_i(x) = S(x)$ for all i,*
(2) *$S_i(x)$ is either a monotone or constant function,*
(3) *The domain of the neural field $[x_{\min}, x_{\max}]$ is covered by the domain of subfunctions, i.e., $d_1 = x_{\min}$ and $d_{N+1} = x_{\max}$.*

Definition 3 means the division of $S(x)$ into N subfunctions $S_i(x)$ (i = 1,…, N) such that each subfunction is either a monotone or constant function. $S_1(x) - S_7(x)$ in Fig. 6a shows an example of the subfunctions for $N = 7$ corresponding to $S(x)$ in Fig. 3a.

Definition 4 *We define Γ_{ij} (i = 1,…, N, j = 1,…, N) to be a set of $(a, \hat{S})$ such that there exist x_1 and x_2 satisfying the following relations:*

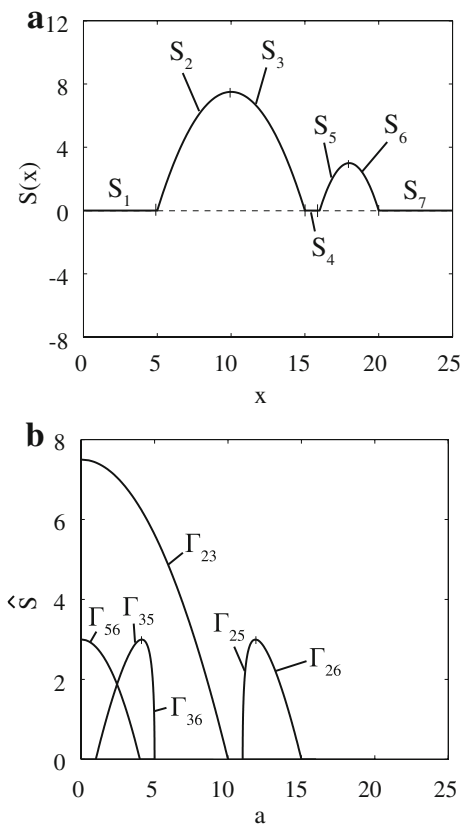

Fig. 6 The way of plotting the $a - \hat{S}$ curve. **a** According to Definition 3, the subfunctions $S_1(x) - S_7(x)$ are constructed from function $S(x)$ in Fig. 3a such that each subfunction is either a monotone or constant function. **b** The $a - \hat{S}$ curve has been drawn by plotting Γ_{ij} (i = 1,…, 7, j = 1,…, 7) by using Theorem 5 from the subfunctions $S_1(x) - S_7(x)$. The line of $\hat{S} = 0$ contains Γ_{ij} for many pairs of i, j, but their labels are omitted

$$(1)\quad x_1 \in D_i, \quad x_2 \in D_j, \tag{B.1}$$

$$(2)\quad x_1 < x_2, \tag{B.2}$$

$$(3)\quad S_i(x_1) = S_j(x_2) = \hat{S}, \tag{B.3}$$

$$(4)\quad a = x_2 - x_1, \tag{B.4}$$

where $D_i \equiv [d_i, d_{i+1}]$ *is the domain of the subfunction* $S(x)$.

From Definitions 1 and 4, we can find that Γ_{ij} is a subset of the $a - \hat{S}$ curve and that the $a - \hat{S}$ curve is described as $\bigcup_{i,j} \Gamma_{ij}$.

Definition 5 *Let* $S_{Li}^{-1}(S)$ *and* $S_{Hi}^{-1}(S)$ *be functions such that*

$$S_{Li}^{-1}(S) = \begin{cases} S_i^{-1}(S), & \text{if } S_i \text{ is a monotone function,} \\ d_i, & \text{if } S_i \text{ is a constant function,} \end{cases} \tag{B.5}$$

$$S_{Hi}^{-1}(S) = \begin{cases} S_i^{-1}(S), & \text{if } S_i \text{ is a monotone function,} \\ d_{i+1}, & \text{if } S_i \text{ is a constant function,} \end{cases} \tag{B.6}$$

where $S_i^{-1}(S)$ *denotes an inverse function of* $S_i(x)$.

From the above definitions, we have the following theorem that gives the explicit description of Γ_{ij}.

Theorem 5 *Let* R_i *be the range of a subfunction* $S_i(x)$. *Then,* Γ_{ij} *is described as follows:*

(1) *When both* S_i *and* S_j $(i < j)$ *are monotone functions and* $R_i \cap R_j \neq \phi$,

$$\Gamma_{ij} = \left\{ (a, \hat{S}) | a = S_j^{-1}(\hat{S}) - S_i^{-1}(\hat{S}),\ a > 0,\ \hat{S} \in R_i \cap R_j \right\}, \tag{B.7}$$

(2) *When* S_i *and/or* S_j $(i \leq j)$ *are constant functions and* $R_i \cap R_j \neq \phi$,

$$\Gamma_{ij} = \left\{ (a, \hat{S}) | a \in [S_{Lj}^{-1}(S_c) - S_{Hi}^{-1}(S_c),\ S_{Hj}^{-1}(S_c) - S_{Li}^{-1}(S_c)],\ a > 0,\ \hat{S} = S_c \right\}, \tag{B.8}$$

where S_c is defined such that $\{S_c\} = R_i \cap R_j$,

(3) *Otherwise,* $\Gamma_{ij} = \phi$.

Proof of Theorem 5 We can prove $\Gamma_{ij} = \phi$ from Definition 4 in case of (1) $i > j$, (2) $R_i \cap R_j \neq \phi$, and (3) S_i is a monotone function and $i = j$. Thus, by excluding these cases, we consider the following five cases,

Case A: Both S_i and S_j are monotone functions, $i < j$, and $R_i \cap R_j \neq \phi$,
Case B: S_i is a monotone function, S_j is a constant function, $i < j$, and $R_i \cap R_j \neq \phi$,
Case C: S_i is a constant function, S_j is a monotone function, $i < j$, and $R_i \cap R_j \neq \phi$,
Case D: S_i is a constant function and $i = j$,
Case E: Both S_i and S_j are constant functions, $i < j$, and $R_i \cap R_j \neq \phi$.

Then, for each case, Γ_{ij} is given by the following lemma. (Proof of the lemma is given later.)

Lemma 1 *Let* S_{ci} *be the value of a subfunction* $S_i(x)$ *when* $S_i(x)$ *is a constant function. Then, for each case,* Γ_{ij} *is described as follows:*

$$\Gamma_{ij} = \left\{ (a, \hat{S}) | a = S_j^{-1}(\hat{S}) - S_i^{-1}(\hat{S}),\ a > 0,\ \hat{S} \in R_i \cap R_j \right\} \text{ for Case A,} \tag{B.9}$$

$$\Gamma_{ij} = \left\{ (a, \hat{S}) | a \in [d_j - S_i^{-1}(S_{cj}),\ d_{j+1} - S_i^{-1}(S_{cj})],\ a > 0,\ \hat{S} = S_{cj} \right\} \text{ for Case B,} \tag{B.10}$$

$$\Gamma_{ij} = \left\{ (a, \hat{S}) | a \in [S_j^{-1}(S_{ci}) - d_{i+1},\ S_j^{-1}(S_{ci}) - d_i],\ a > 0,\ \hat{S} = S_{ci} \right\} \text{ for Case C,} \tag{B.11}$$

$$\Gamma_{ij} = \left\{ (a, \hat{S}) | a \in (0, d_{i+1} - d_i],\ \hat{S} = S_{ci} \right\} \text{ for Case D,} \tag{B.12}$$

$$\Gamma_{ij} = \left\{ (a, \hat{S}) | a \in [d_j - d_{i+1},\ d_{j+1} - d_i],\ a > 0,\ \hat{S} = S_{ci} \right\} \text{ for Case E.} \tag{B.13}$$

From Lemma 1, we can see that Γ_{ij} for Cases A is the same as (B.7), and that Γ_{ij} for Cases B-E are summarized as (B.8) by using the notations of S_{Li}^{-1} and S_{Hi}^{-1} in Definition 5, so that we obtain Theorem 5. □

The proof of Lemma 1 is given as follows.

Proof of Lemma 1 Since proofs of Cases A − E are similar, we show only proof of Case A and omit proofs of the other cases.

If $(a, \hat{S}) \in \Gamma_{ij}$, there exist x_1 and x_2 that satisfy (B.1)–(B.4) from the definition of Γ_{ij}. We can find $\hat{S} \in R_i \cap R_j$ from (B.3) and $a = S_j^{-1}(\hat{S}) - S_i^{-1}(\hat{S})$ from (B.3) and (B.4). $a > 0$ also holds from (B.2) and (B.4), so that

$$(a, \hat{S}) \in \left\{ (a, \hat{S}) | a = S_j^{-1}(\hat{S}) - S_i^{-1}(\hat{S}),\ a > 0,\ \hat{S} \in R_i \cap R_j \right\}. \tag{B.14}$$

On the contrary, if (B.14) holds, we can obtain (B.1)–(B.4) by setting $x_1 = S_i^{-1}(\hat{S})$ and $x_2 = S_j^{-1}(\hat{S})$. Thus, we have $(a, \hat{S}) \in \Gamma_{ij}$. □

Since the $a - \hat{S}$ curve is $\bigcup_{i,j} \Gamma_{ij}$ as stated above, we can draw the $a - \hat{S}$ curve by plotting points $(a, \hat{S}) \in \Gamma_{ij}$ for

every i, j with $\Gamma_{ij} \neq \phi$ by using Theorem 5. Figure 6b shows how the $a - \hat{S}$ curve is composed of Γ_{ij}, where each curve Γ_{ij} has been obtained from $S_i(x)$ and $S_j(x)$ depicted in Fig. 6a.

Appendix C: The method for finding solutions of the steady condition 1

Here we show how the solutions of the steady condition 1 can be obtained when the intersections of the $a - \hat{S}$ curve with $Y(a)$ are given. All the definitions in Appendix B (Definitions 2–5) are also used in this appendix.

As mentioned in Appendix B, the $a - \hat{S}$ curve is written as $\bigcup_{i,j} \Gamma_{ij}$ by using Γ_{ij} in Definition 4. Therefore, when a point $(a, \hat{S})$ lies on the $a - \hat{S}$ curve, $(a, \hat{S}) \in \Gamma_{ij}$ holds for some pair of i, j, and there exist x_1 and x_2 satisfying (B.1)–(B.4). Hence, we denote a set of these variables (x_1, x_2) by $\Theta_{ij}[a, \hat{S}]$. The following theorem shows the explicit description of $\Theta_{ij}[a, \hat{S}]$.

Theorem 6 *$\Theta_{ij}[a, \hat{S}]$ is given as follows:*

(1) *When S_i and/or S_j are monotone functions,*

$$\Theta_{ij}[a, \hat{S}] = \left\{(x_1, x_2) | x_1 = \max\left(S_{Li}^{-1}(\hat{S}),\, S_{Lj}^{-1}(\hat{S}) - a\right),\; x_2 = x_1 + a\right\}, \tag{C.1}$$

(2) *When both S_i and S_j are constant functions,*

$$\Theta_{ij}[a, \hat{S}] = \left\{(x_1, x_2) | x_1 \in \left[\max\left(S_{Li}^{-1}(\hat{S}),\, S_{Lj}^{-1}(\hat{S}) - a\right),\, \min\left(S_{Hi}^{-1}(\hat{S}),\, S_{Hj}^{-1}(\hat{S}) - a\right)\right],\; x_2 = x_1 + a\right\}, \tag{C.2}$$

where S_i and S_j are the subfunctions defined in Definition 3. S_{Li}^{-1} and S_{Hi}^{-1} are the functions defined in Definition 5.

Proof of Theorem 6 We present the following lemma. (The proof of this lemma is shown later.)

Lemma 2 *Consider the same classification as Cases A–E shown in proof of Theorem 5 in Appendix B, then $\Theta_{ij}[a, \hat{S}]$ for each case is given as follows:*

$$\Theta_{ij}[a, \hat{S}] = \left\{(x_1, x_2) | x_1 = S_i^{-1}(\hat{S}),\; x_2 = x_1 + a\right\} \quad \text{for Case A,} \tag{C.3}$$

$$\Theta_{ij}[a, \hat{S}] = \left\{(x_1, x_2) | x_1 = S_i^{-1}(\hat{S}),\; x_2 = x_1 + a\right\} \quad \text{for Case B,} \tag{C.4}$$

$$\Theta_{ij}[a, \hat{S}] = \left\{(x_1, x_2) | x_1 = S_j^{-1}(\hat{S}) - a,\; x_2 = x_1 + a\right\} \quad \text{for Case C,} \tag{C.5}$$

$$\Theta_{ij}[a, \hat{S}] = \left\{(x_1, x_2) | x_1 \in [d_i, d_{i+1} - a],\; x_2 = x_1 + a\right\} \quad \text{for Case D,} \tag{C.6}$$

$$\Theta_{ij}[a, \hat{S}] = \left\{(x_1, x_2) | x_1 \in [\max(d_i, d_j - a), \min(d_{i+1},\, d_{j+1} - a)],\; x_2 = x_1 + a\right\} \quad \text{for Case E,} \tag{C.7}$$

where $[d_i, d_{i+1}]$ is the domain of the subfunction $S_i(x)$ in Definition 3.

If we use the notations of S_{Li}^{-1} and S_{Hi}^{-1} in Definition 5, then Cases A–E in Lemma 2 can be summarized as Theorem 6. □

The proof of Lemma 2 is given as follows.

Proof of Lemma 2 Since proofs of Cases A–E are similar, we show only proof of Case A and omit the proofs of the other cases. From $(a, \hat{S}) \in \Gamma_{ij}$ and Lemma 1, we have

$$a = S_j^{-1}(\hat{S}) - S_i^{-1}(\hat{S}), \tag{C.8}$$

$$a > 0, \tag{C.9}$$

$$\hat{S} \in R_i \cap R_j. \tag{C.10}$$

If $(x_1, x_2) \in \Theta_{ij}[a, \hat{S}]$, we find $x_1 = S_i^{-1}(\hat{S})$ and $x_2 = S_j^{-1}(\hat{S})$ from (B.3). By using (C.8), we have $x_2 = x_1 + a$, so that

$$(x_1, x_2) \in \left\{(x_1, x_2) | x_1 = S_i^{-1}(\hat{S}),\; x_2 = x_1 + a\right\}. \tag{C.11}$$

On the contrary, if (C.11) holds, we can prove that (B.1)–(B.4) also hold by using (C.8) and (C.9). Thus, we obtain $(x_1, x_2) \in \Theta_{ij}[a, \hat{S}]$. □

Consider an intersection point (a_k^*, S_k^*) of the $a - \hat{S}$ curve with $Y(a)$ as in Step 1 of the graphic analysis method. Let us define i_k and j_k to be the integers satisfying $(a_k^*, S_k^*) \in \Gamma_{i_k j_k}$, and set $\Theta_k = \Theta_{i_k j_k}[a_k^*, S_k^*]$. Then, from the definition of $\Theta_{ij}[a, \hat{S}]$, we can find $a_k^* = x_{2,k}^* - x_{1,k}^*$ and $S(x_{1,k}^*) = S(x_{2,k}^*) = S_k^*$ for $(x_{1,k}^*,\, x_{2,k}^*) \in \Theta k$. Since we can have the following corollary from Theorem 3, $(x_1^*, x_2^*) \in \bigcup_k \Theta_k$ are the solutions of the steady condition 1 in Theorem 1.

Corollary 1 *The steady condition 1 holds for x_1^*, x_2^* if and only if*

$$(x_1^*, x_2^*) \in \bigcup_k \Theta_k.$$

Proof of Corollary 1 If the steady condition 1 holds for x_1^*, x_2^* ($x_1^* < x_2^*$), the point (a^*, S^*) with $a^* = x_2^* - x_1^*$ and $S^* = S(x_2^*) - S(x_1^*)$ is an intersection of the $a - \hat{S}$ curve with $Y(a)$ from Theorem 3.

We find $S_i(x_1^*) = S_j(x_2^*) = S^*$ with i, j satisfying $x_1^* \in D_i$ and $x_2^* \in D_j$, where S_i and D_i ($i = 1, \ldots, N$) denote the subfunction and its domain in Definition 3. Hence, $(a^*, S^*) \in \Gamma_{ij}$ holds from Definition 4. Since $a^* = a_k^*$, $S^* = S_k^*$, $i = i_k$, and $j = j_k$ hold for some k, we can obtain

$$x_1^* \in D_{i_k}, \quad x_2^* \in D_{j_k}, \tag{C.12}$$

$$S_{i_k}(x_1^*) = S_{j_k}(x_2^*) = S_k^*, \tag{C.13}$$

$$a_k^* = x_2^* - x_1^*. \tag{C.14}$$

Therefore, we can find $(x_1^*, x_2^*) \in \Theta_k$.

On the contrary, if $(x_1^*, x_2^*) \in \Theta_k$ holds for some k, (C.13) and (C.14) hold. Since (a_k^*, S_k^*) lies on an intersection of the $a - \hat{S}$ curve with $Y(a)$, we obtain the steady condition 1 from Theorem 3. □

Since the elements of $\Theta_k = \Theta_{i_k j_k}[a_k^*, S_k^*]$ can be obtained by using Theorem 6 for each k, we can actually find the solutions of the steady condition 1. Note that, Theorem 6 indicates that, if both S_{i_k} and S_{j_k} are constant functions, Θ_k contains infinite number of elements. Thus, in this case, we need to pick up some elements $(x_{1,k}^*, x_{2,k}^*) \in \Theta_k$ by the required accuracy in order to plot $G[x; x_{1,k}^*, x_{2,k}^*]$ in Step 2 of the graphic analysis method.

References

1. Wilson HR, Cowan JD (1973) A mathematical theory of the functional dynamics of cortical and thalamic nervous tissue. Kybernetik 13:55–80
2. Amari S (1977) Dynamics of pattern formation in lateral-inhibition type neural fields. Biol Cybern 27:77–87
3. Werner H, Richter T (2001) Circular stationary solutions in two-dimensional neural fields. Biol Cybern 85:211–217
4. Laing CR, Troy WC, Gutkin B, Ermentrout GB (2002) Multiple bumps in a neuronal model of working memory. SIAM J Appl Math 63:62–97
5. Laing CR, Troy WC (2003) Two-bump solutions of Amari-type models of neuronal pattern formation. Physica D 178:190–218
6. Enculescu M, Bestehorn M (2003) Activity dynamics in nonlocal interacting neural fields. Phys Rev E 67:041904
7. Hutt A, Bestehorn M, Wennekers T (2003) Pattern formation in intracortical neural fields. Network 14:351–368
8. Owen MR, Laing CR, Coombes S (2007) Bumps and rings in a two-dimensional neural field: splitting and rotational instabilities. New J Physics 9:378
9. Pinto DJ, Ermentrout GB (2001) Spatially structured activity in synaptically coupled neuronal networks: II. Lateral inhibition and standing pulses. SIAM J Appl Math 62:226–243
10. Ben-Yishai R, Hansel D, Sompolinsky H (1997) Traveling waves and the processing of weakly tuned inputs in a cortical network module. J Comput Neurosci 4:57–77
11. Bressloff PC (2001) Traveling fronts and wave propagation failure in an inhomogeneous neural network. Physica D 155:83–100
12. Pinto DJ, Ermentrout GB (2001) Spatially structured activity in synaptically coupled neuronal networks: I. Traveling fronts and pulses. SIAM J Appl Math 62:206–225
13. Amari S (1989) Dynamical stability of formation of cortical maps. In: Arbib MA, Amari SI (eds) Dynamic interactions in neural networks: models and data. Springer, New York, pp 15–34
14. Giese MA (1999) Dynamic neural field theory for motion perception. Kluwer, Boston
15. Kubota S, Aihara K (2005) Analyzing global dynamics of a neural field model. Neural Process Lett 21:133–141
16. Coombes S (2005) Waves, bumps, and patterns in neural field theories. Biol Cybern 93:91–108
17. Ermentrout B (1998) Neural networks as spatio-temporal pattern-forming systems. Rep Prog Phys 61:353–430
18. Fender D, Julesz B (1967) Extension of Panum's fusional area in binocularly stabilized vision. J Opt Soc Am 57:819–830
19. Ichihara-Takeda S, Funahashi S (2007) Activity of primate orbitofrontal and dorsolateral prefrontal neurons: task-related activity during an oculomotor delayed-response task. Exp Brain Res 181:409–425
20. Tsujimoto S, Sawaguchi T (2004) Properties of delay-period neuronal activity in the primate prefrontal cortex during memory- and sensory-guided saccade tasks. Eur J NeuroSci 19:447–457
21. Durstewitz D, Seamans JK, Sejnowski TJ (2000) Neurocomputational models of working memory. Nat Neurosci suppl 3:1184–1191
22. Tegner J, Compte A, Wang XJ (2002) The dynamical stability of reverberatory neural circuits. Biol Cybern 87:471–481
23. Wang (2001) Synaptic reverberation underlying mnemonic persistent activity. Trends Neurosci 24:455–463
24. Tsunoda K, Yamane Y, Nishizaki M, Tanifuji M (2001) Complex objects are represented in macaque inferotemporal cortex by the combination of feature columns. Nat Neurosci 4:832–838
25. Yamane Y, Tsunoda K, Matsumoto M, Phillips AN, Tanifuji M (2006) Representation of the spatial relationship among object parts by neurons in macaque inferotemporal cortex. J Neurophysiol 96:3147–3156
26. Zhang (1996) Representation of spatial orientation by the intrinsic dynamics of the head-direction cell ensemble: a theory. J Neurosci 16:2112–2126
27. Bassett JP, Tullman ML, Taube JS (2007) Lesions of tegmento-mammillary circuit in the head direction system disrupt the head direction signal in the anterior thalamus. J Neurosci 27:7564–7577
28. Ben-Yishai R, Bar-Or RL, Sompolinsky H (1995) Theory of orientation tuning in visual cortex. Proc Natl Acad Sci USA 92:3844–3848